Publications of the Astronomical Society of the Pacific
**104:** 270–277, 1992 April

# Precision Radial Velocities with an Iodine Absorption Cell

GEOFFREY W. MARCY[1]

Astronomy Department, University of California, Berkeley, California 94720
Electronic mail: gmarcy@ucbast.berkeley.edu

R. PAUL BUTLER

Astronomy Department, University of Maryland, College Park, Maryland 20742
Electronic mail: paul@astro.umd.edu

*Received 1991 October 24; accepted 1992 January 17*

**ABSTRACT.** We have used gaseous iodine for generating reference absorption lines in stellar spectra taken at high resolution. A major advance involves the use of a fast echelle spectrograph and a $2048 \times 2048$ CCD which acquires the near-ultraviolet, the entire visible, and the near-infrared spectrum in a single exposure. The superimposed iodine lines provide both a highly precise wavelength scale (calibrated with a Fourier-transform spectrum) and a specification of the spectrograph PSF *in situ* over the entire echelle format. Test observations of three solar-type stars exhibit a velocity scatter of less than 25 m s$^{-1}$ over a 1-yr duration, and only 1/5 of the available spectrum has been employed in the analysis to date. Velocity precision of 50 m s$^{-1}$ can be achieved for magnitude $V=12$ in 1 h exposures on a 3-m telescope. We discuss an on-going project to detect brown-dwarf and planetary companions to F-, G-, K-, and M-type main-sequence stars, designed to complement other efforts. The current velocity precision permits detection of companions with masses as low as 3 $M_{\rm Jup}$ located up to 5 AU from the star. We also discuss the use of precision velocities in revising Cepheid distances.

## 1. INTRODUCTION

The conventional technique for measuring Doppler shifts in optical spectra involves determination of a wavelength scale by exposures of a reference lamp that provides lines of known wavelength. Experience shows that the errors in Doppler shift measurements are typically greater than those expected from photon statistics alone and are often systematic. These errors are caused by the different optical paths traveled by the stellar beam and the reference-lamp beam. Indeed, the two exposures are usually obtained at different times so that spectrograph flexure, detector movement, different photocenters at the slit, and dissimilar illumination of imperfect spectrograph optics cause spurious shifts as well as distortions in both the dispersion and the PSF. To our knowledge the best precision achieved by traditional techniques is about 200 m s$^{-1}$ (Marcy and Benitz 1989; Latham et al. 1989; Duquennoy and Mayor 1991).

The solution offered by Griffin and Griffin (1973) is to pass the starlight through an absorbing medium before entry into the spectrometer, thereby superimposing reference absorption lines that experience the same instrumental shifts and distortions as the stellar spectrum. This general approach, with variations, has been tried successfully by several groups: Campbell and Walker (1979), Smith (1983), Cochran and Hatzes (1990), and Smith et al. (1987), the latter employing a Fabry–Perot to provide the reference fiducials. For precise Doppler measurements over time scales of one night, several groups have successfully employed multiple optical fibers to achieve conformity of all beams entering the spectrograph (Heacox 1988; Ramsey et al. 1990; Brown 1990).

All groups have demonstrated a velocity precision better than $\sim$25 m s$^{-1}$ (although better on short time scales) which approaches the intrinsic astrophysical limit imposed by long-time-scale changes in turbulence on the stellar surface (Deming et al. 1987; Wallace et al. 1988). Yet all groups are limited to the brightest stars (typically, $V<6$) because of the need for extremely high signal-to-noise ratios in the spectra. For stars having $V\approx 6$, the typical exposure time on a 4-m class telescope is 1 hr, limiting the number of stars that can be monitored. Many classes of stars are currently excluded from precision velocity study: only a handful of K dwarfs and Cepheids are brighter than $V=6$, and no RR Lyraes or M dwarfs are accessible. The latter is particularly unfortunate because low-mass stars, compared to G dwarfs, would be perturbed to a greater extent by a substellar companion of given mass and orbital radius. Also, such interesting cases as members of nearby open clusters are completely inaccessible.

The obvious way to improve the magnitude limit is to acquire the largest wavelength band possible and to use a detector with lowest possible read-out noise. Here we describe an effort to use a large-format echelle/CCD spectrometer with an absorbing medium of gaseous iodine designed to provide wavelength reference lines over a wide portion of the echelle format. We discuss applications of precision velocities to the search for low-mass companions of stars and to the Cepheid distance scale.

## 2. CONSIDERATIONS FOR PRECISE DOPPLER MEASUREMENTS

To achieve Doppler precision limited by photon statistics, several sources of systematic errors must be addressed in all grating spectrometers. Foremost among these is movement of the photocenter of the telescope pupil at the spectrograph slit. This effect can cause spurious spectral shifts as large as the projected slit width, usually several pixels on the detector. In practice the actual error amounts to about 1/10 of the projected slit width for well-guided exposures. Mechanical instabilities of the spectrograph structure, even in isolated and stationary habitats, can cause spurious shifts which are typically a non-negligible fraction of one pixel. (Even such innocent effects as the evaporation of liquid coolant in a dewar changes local

[1]On leave from San Francisco State University.

torques and stresses.) Thermal variations may induce alterations in the figure of optics, the groove spacing of gratings, the detector shape and sensitivity, and the refraction index of air (Brown 1990). All of the above nemeses can cause not only spurious shifts but also changes in dispersion and the spectrograph PSF.

Indeed, the two-dimensional spectrograph PSF may change with wavelength and with time. The focusing of the spectrograph each observing session may cause significant variations in the asymmetry as well as width of the PSF. The PSF is also vulnerable to optical imperfections in the spectrograph, especially to the fast optics of some cameras. Thus, small displacements of the collimated beam may significantly alter the PSF. This implies that changes in the alignment of optics and vignetting of any beams in the telescope or spectrograph will change the PSF. The effects of changes in the PSF can be estimated by the following rule of thumb. The spurious Doppler shift, measured in units of the width of the PSF, is roughly equal to 1/2 of the fractional change in the intensity of the PSF profile where an asymmetry occurs. Thus if a wing of a PSF, which has a width of 2 pixels, changes by, say, 5% of peak intensity, systematic errors of $\sim$0.1 pixel in the derived Doppler shift can result. The actual error will depend, of course, on the precise profile variation and the Doppler algorithm used.

Precise Doppler measurements also require careful determination of the topocentric velocity relative to the Solar-System barycenter which varies by about 2 m s$^{-1}$ per minute. Thus a flux-weighted midpoint of the time of observation must be determined. In addition, the data reduction requires attention to the summation of the spectrograph PSF perpendicular to dispersion, scattered light as a function of wavelength, and pixel sampling effects near the Nyquist frequency.

We elected to construct an instrument for precise velocities based on an absorption-cell concept, similar in principal to that of Campbell and Walker (1979). The motivation for this choice over a fiber or Fabry–Perot design derived from a desire for a system having exceptionally high throughput, large wavelength coverage, and unquestioned velocity stability over time scales of several decades.

## 3. THE ECHELLE SPECTROGRAPH AND IODINE CELL

During the past 2 yr, we carried out tests of precise Doppler measurements using the Coudé echelle spectrograph ("Hamilton") at the Lick Observatory 3-m telescope. This spectrometer (Vogt 1987) gathers spectrum from 3800 to 9500 Å, parcelled over 100 spectral orders on a 2048$\times$2048 Ford Aerospace CCD detector (Geary et al. 1990). For comparison, Campbell et al. (1988) gather 100 Å of spectrum at a spectral resolution identical to ours, $\lambda/\Delta\lambda = 40000$. The Lick echelle spectrometer has high throughput (all optics are overcoated), and the detector has high quantum efficiency (about 40%) and low read-out noise (6 $e$- per pixel). Stars of magnitude $V = 13$ are routinely observed with this instrument. A Doppler shift of 0.01 pixel corresponds to 25 m s$^{-1}$.

The challenge is to find an absorbing medium that can provide sharp, stable wavelength fiducials over the huge wavelength range of the echelle format. An extensive search shows that the medium of choice is gaseous iodine (cf. Koch and Wohl 1984) which offers the following advantages: (1) it has a strong line absorption coefficient, requiring a path length of only a few centimeters at pressures much less than 1 atm; (2) wavelength coverage from 5000 to 6300 Å with at least two "features" per Å; (3) it is chemically stable, only slightly corrosive, and nonlethal. (Thanks are due to chemists, Dr. G. Herzberg and Dr. H. Okabe, for valuable suggestions on absorbing media.) An atlas of the spectrum of molecular iodine and a discussion of its origin is provided by Gerstenkorn and Luc (1978).

For comparison, the HF molecule used by Campbell et al. (1988) requires a meter-long absorption cell at 100 C, provides lines over only 100 Å of spectrum, is chemically reactive with glass, and is an odorless lethally corrosive gas. The HF choice was motivated by a desire to avoid blends with stellar lines. Molecular iodine produces omnipresent blends that must be treated by modeling the composite spectrum as described in Sec. 4.

The $I_2$ absorption cell is cylindrical, with a length of 10 cm and diameter of 5 cm and has flat ($2\lambda$) Pyrex windows that are antireflection coated. The windows are sealed by a glass blower onto the Pyrex cylindrical body. Before introduction of $I_2$, a thin Pyrex tube was puncture-melted into the side of the body to provide access to the cell. The cell was then washed with a strong acid solution, rinsed clean with distilled water, and finally rinsed with 200 proof ethanol to facilitate drying. After the cell had completely dried, a small pure iodine fragment was rolled into the cell via the thin tube. A vacuum pump was attached to the side tube, and after the cell was evacuated the glass blower flame-pinched the tube near its end, with the pump still running. The iodine fragment was then rolled from the cell body into the tube, now closed off. The side tube was then placed in a water bath heated to 34.8 C. The absorption cell was heated to a temperature much greater than 34.8 C so that the iodine vapor pressure was set by the water bath. The side tube was then flame-pinched off from the absorption cell without allowing any iodine vapor to escape or any air to leak in. The cell is thus left with gaseous molecular iodine at a pressure of about 1/100 atm.

The absorption cell is mounted about 10 cm in front of the spectrograph slit, with its axis coincident with the telescope axis. Thermal insulation, consisting of foam rubber of thickness 1 cm, is permanently placed around the body of the cylinder. The entire system is temperature controlled at 50$\pm$0.1 C, which ensures that all iodine is in vapor form during operation and that the pressure broadening of the $I_2$ lines does not change. Once in place, the absorption cell requires no operator intervention during the night. Long term, it requires almost no maintenance (occasional replacement of thermal insulation and probes), and the number of $I_2$ molecules remains fixed indefinitely, as verified by the constancy of line depths during 2 yr of operation.

A representative 5 Å portion of the $I_2$ absorption spectrum is shown in Fig. 1, obtained at a resolution of 400000 and S/N = 1000 with the FTS at the McMath telescope of the National Solar Observatories at Kitt Peak. Clearly, the $I_2$ spectrum consists of a high density of features, typically several per Å, which overlap even at infinite resolution. The features are so narrow that considerable power exists beyond the Nyquist frequency when sampled by the Lick echelle. Features having a depth greater than 10% exist from 5000 to 6300 Å. At longer wavelengths the lines become weaker and contain little information. The density of the $I_2$ lines is sufficiently high that they form blends with

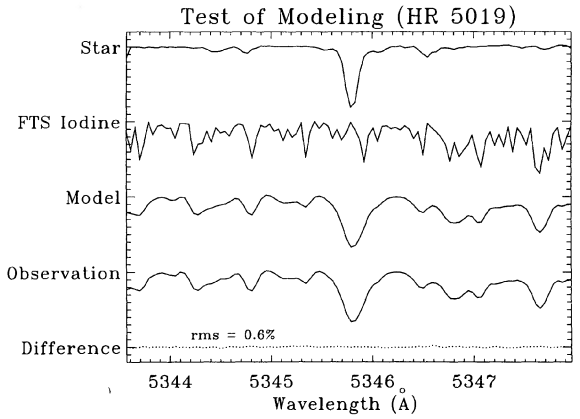


FIG. 1—The modeling process. Top: $I_s$, 5 Å of bare, deconvolved stellar spectrum (HR 5019, G6 V). Second: $T_{I_2}$, FTS determination of transmission of $I_2$ cell. Third: Model: $(I_s \cdot T_{I_2}) \otimes$ PSF. Fourth: Observation of star passed through $I_2$ cell. Bottom: Difference between the model and observation. The model and observation differ by 0.6%, rms.

all stellar lines.

The Lick echelle is configured specially for the acquisition of precise velocities. Directly over the collimator mirror is placed a black mask that blocks the outer 2.5 cm of the 20-cm telescope pupil. In addition, a central black obstruction blocks light in a region about 1 cm larger than the shadow of the central obstruction of the 3-m telescope. This central obstruction, the "Felix mask," has small-scale features caused by the mount, spider, and hinges of the tertiary telescope mirror. The entire collimator mask ensures that small movements of the telescope pupil, with time and hour angle, will not cause corresponding movement in the collimated beam traversing the remainder of the spectrograph. However, the mask causes a light loss of $\sim$30%. Another feature of the setup involves use of a programmed algorithm for focusing the CCD, based on Gaussian fits to five thorium lines. The focus procedure is performed each night just before observing. The CCD and grating are always positioned such that the thorium lines hit precisely the same pixels each run. The flat-field lamp is carefully positioned in front of the slit to ensure uniform illumination of the collimator mask. Finally the axis of the iodine cell is made coincident with the telescope optical axis by use of a laser.

## 4. THE DOPPLER ANALYSIS

In practice, starlight passes through the $I_2$ absorption cell, thereby superimposing $I_2$ lines on the stellar spectrum, creating blends of the two. The resulting composite spectrum enters the echelle spectrometer where it is convolved with the instrumental profile and dispersed nearly linearly in wavelength on the CCD. *The principle of the analysis is that the observed shift of a stellar spectrum consists of two parts, the actual Doppler shift and a small spurious shift due to instrumental effects* mentioned in Sec. 2. These spurious shifts are represented entirely by the shifts of the $I_2$ lines that form in the absorption cell which is at rest relative to the observatory. Therefore, the analysis consists of determining this spurious, instrumental shift of the $I_2$ lines, which is then applied as a correction to the observed shift of the stellar spectrum. The result is the Doppler shift of the star. Note that one obtains Doppler shifts relative to the stellar template, not absolute velocities. However, systematic errors historically due to the different optical paths of the stellar and calibration beams are eliminated.

The large amount of Doppler information contained in these echelle spectra (about 300 moderately deep stellar absorption lines) requires an analysis that is general enough to treat all blends and instrumental effects without operator intervention and yet yields the desired precision of about 15 m s$^{-1}$ for at least 20 yr. We present here the Doppler analysis that we are continuing to develop.

A rigorous Doppler analysis must consist of a full model of the observed spectrum, including the shift of the stellar spectrum, the shift of the superimposed iodine lines, and the PSF of the spectrograph. We plan to model the observed composite spectrum by using two functions of wavelength, namely the bare, intrinsic stellar spectrum, $I_s$, and the transmission function $T_{I_2}$, of the $I_2$ absorption cell. The product of these two must be convolved with the PSF and integrated over CCD-pixel bins to reproduce the observed spectrum. Trial shifts of the stellar and $I_2$ spectrum will yield a best fit to the observed composite spectrum.

We model the spectrum (taken through the absorption cell), $I_{\rm obs}(\lambda)$, as

$$I_{\rm obs}(\lambda) = k[I_s(\lambda+\Delta\lambda_s)T_{I_2}(\lambda+\Delta\lambda_{I_2})] \otimes \text{PSF}. \quad (1)$$

Here, $\Delta\lambda_s$ and $\Delta\lambda_{I_2}$ are the shifts of the star spectrum and iodine transmission function, respectively, and the symbol $\otimes$ represents convolution. The constant $k$ is proportional to the exposure level of the observation. In operation, $\Delta\lambda_s$, $\Delta\lambda_{I_2}$, and $k$ are determined by least-squares fitting to the observed, composite spectrum, $I_{\rm obs}$.

The final, corrected Doppler shift, $\Delta\lambda$, is simply given by

$$\Delta\lambda = \Delta\lambda_s - \Delta\lambda_{I_2}, \quad (2)$$

which is converted to a velocity by the Doppler formula:

$$\lambda = \lambda_0 \frac{(1+\beta\cos\theta)(1+\rho_g)}{n(1-\beta^2)^{1/2}}. \quad (3)$$

Here, $\lambda_0$ is the rest wavelength, $\lambda = \lambda_0 + \Delta\lambda$, $\beta = v/c$, topocentric, $\theta$ is the angle between line of sight and topocentric velocity vector of star, $\rho_g$ is the gravitational redshift of stellar beam, and $n$ is the index of refraction of air at the spectrograph.

Ignoring $\rho_g$ and $n$ causes errors in relative stellar velocities of less than 1 m s$^{-1}$. The special relativistic terms in Eq. (3) correspond to changes in $v$ of several m s$^{-1}$ (for a given $\Delta\lambda$), and therefore are significant here.

The two necessary functions in Eq. (1), $I_s$ and $T_{I_2}$, are obtained *a priori* as follows. $I_s$ is obtained by observing each program star *without* the $I_2$ cell in place. This gives $I_s \otimes$ PSF, not $I_s$ as desired. We deconvolve the PSF from the spectrum using either a Fourier division or the Jansson method (Gilliland 1990), both yielding satisfactory test results. The $I_2$-cell transmission function, $T_{I_2}$, is obtained by transporting the absorption cell to Kitt Peak National Observatory and using the Fourier-Transform Spectrometer which gives a resolution of 400 000. The resulting $I_2$ transmission function is conveniently both oversampled and fully resolved, with no appreciable PSF of its own, thus ideally representing $T_{I_2}$. This FTS $I_2$ spectrum is avail-

able to anyone upon request.

The iodine transmission function, $T_{I_2}$, provides two other important elements in the modeling process. First, the FTS spectrum carries a highly precise *absolute, vacuum* wavelength scale, accurate to 1:$10^8$. Thus, each Lick Observatory spectrum taken through the $I_2$ cell automatically carries a superimposed wavelength scale having precision comparable to the best fundamental laboratory wavelengths. Second, the FTS iodine spectrum provides a reference spectrum with which to determine the PSF of the Lick echelle spectra, as we now describe.

## 5. THE POINT-SPREAD FUNCTION

The determination of the spectrograph PSF represents the final ingredient in Eq. (1) to solve for $\Delta\lambda_s$ and $\Delta\lambda_{I_2}$. Tests with both laser and thorium spectra show that the PSF varies by several percent over the two-dimensional format of the Lick echelle. Also, variations of the PSF with time may occur, owing to, for example: (1) changes in spectrograph focus, (2) movement of the optical axis of the telescope relative to the spectrograph, (3) changes in the charge transfer efficiency of the CCD, (4) nonuniform illumination of the slit, and (5) structural and thermal changes in the spectrograph. *Changes in the PSF will cause systematic shift errors which are different for the stellar and iodine spectra,* as modeled extensively with mock spectra. Thus, these spurious shifts due to a changing PSF do not cancel in Eq. (2). The resulting velocity errors can be as large as 50 m $s^{-1}$.

More specifically, the systematic errors in Doppler shift caused by the PSF arise in the following way. Suppose that the PSF is a Gaussian centered at the origin but contaminated by an enhancement in one wing located several Gaussian widths from the center, so that the peak of the PSF remains at the origin. Consider the convolution of this PSF with two lines, one intrinsically narrower than the PSF and one intrinsically broader, i.e., iodine and stellar lines, respectively. This is indeed the regime of relative widths in which we operate at Lick.

The intrinsically narrow line, when convolved with this PSF, will yield an "observed" profile that is a near replica of the PSF (the convolution of a delta function with the PSF is just the PSF). Thus, its line core will be undisplaced from the original narrow line, but there will be the enhancement in its far wing. The resulting "shift" in the position of the line (due entirely to the PSF asymmetry) depends on the algorithm used to measure line position. For example, one may adopt the minimum of the line profile as the "location" of the line. In this case, the "shift" for this convolved, narrow line will be essentially zero, even though its wings are asymmetric. By comparison, the line that is intrinsically broader than the PSF, when convolved, will exhibit an asymmetry that is more complicated. The convolution process causes a displacement of original line profile at each point in the direction of the asymmetry. Thus, the location of the minimum of the convolved profile will also shift toward the asymmetry. Therefore, an algorithm that measures shift by the location of the profile minimum will detect a nonzero shift, unlike the case for the intrinsically narrow line. Other algorithms we have considered, such as parabolic fits to the core and cross correlation, are susceptible to this differential shift.

Interestingly, an algorithm that measures the first-moment position of convolved lines would yield identical displacements for the broad and narrow lines, namely the precise displacement from the origin of the first moment of the PSF itself. Thus the net error in the Doppler shift would be removed in Eq. (2). However, in practice it is difficult to measure the first moment of a line profile in the presence of weak blends in the line wings. We have therefore elected to incorporate the actual PSF in the shift algorithm to account for the above effects directly.

We determine the PSF as a function of position over the entire CCD format with a completely innovative strategy. Each stellar spectrum, taken through the $I_2$ cell, is divided by a bare "template" spectrum of that star, taken without the $I_2$ cell. This leaves the $I_2$ transmission function convolved with the PSF, $T_{I_2} \otimes$ PSF, to an excellent approximation. In detail, we treat carefully the mutual convolution of stellar and iodine spectra with the PSF, as well as the small relative shifts between observation and template.

With $T_{I_2} \otimes$ PSF, recovered from each observation, we can extract the PSF by using the known transmission function, $T_{I_2}$, obtained with the FTS at Kitt Peak. The extraction can be accomplished by a straightforward nonlinear least-squares approach in which different PSFs are tried until convolution with $T_{I_2}$ yields a best fit with the recovered $T_{I_2} \otimes$ PSF. Since the PSF may be a function of wavelength, we carry out the analysis using small pieces of spectrum (typically $\sim$30 pixels long) at all locations over the echelle. This approach yields the instantaneous PSF for each observation at each wavelength, measured *in situ*. A complete description of this PSF-recovery technique is in progress (Valenti et al. 1992).

One concern in the PSF extraction is the undersampling of the iodine line profiles by the Lick spectrograph and CCD, which has pixels of size 2.5 km $s^{-1}$. The FTS spectrum of iodine shows that the intrinsic iodine features have widths as narrow as 2.0 km $s^{-1}$, less than one pixel width. Thus the iodine lines are both unresolved and undersampled. Much spectral information above the Nyquist frequency is irretrievably lost under such conditions, preventing any hope of rectification by image processing. However, this loss of information does not introduce a systematic error in the iodine shifts as determined by any algorithm, nor does it prevent extraction of the PSF. Indeed, information about the PSF, even above the Nyquist frequency, remains in the iodine CCD spectra because of the large number of lines available to constrain its shape. In our current preliminary Doppler analysis, we integrate the FTS iodine spectrum over individual CCD pixels and employ the result as the intrinsic iodine transmission function, $T_{I_2}$, in Eq. (1). This discrete function is then shifted in Fourier space by trial amounts to determine $\Delta\lambda_{I_2}$, as described in Sec. 6. A superior treatment would involve applying trial shifts to the finely sampled, original FTS spectrum, and integrating over CCD pixels only after shifting.

## 6. APPLICATION AND TESTS OF THE DOPPLER ANALYSIS

Equation (1) is solved numerically for $\Delta\lambda_s$ and $\Delta\lambda_{I_2}$ by a least-squares fit. In practice, trial shifts of $I_s$ and $T_{I_2}$ are accomplished by rotating the phase of the Fourier transforms and then transforming back. This effectively performs an interpolation between pixels, superior to that by cubic spline, permitting the spectra to be shifted by noninteger pixel amounts. Small sections of the observed spec-

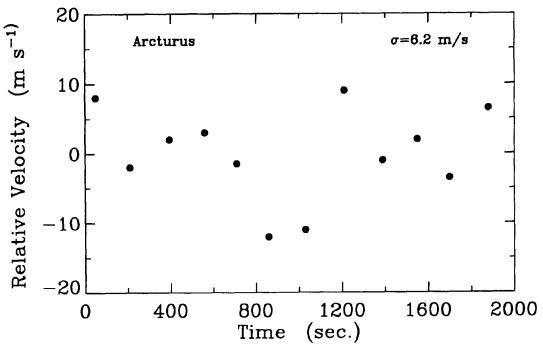


FIG. 2—Velocity test of Arcturus. 35 separate exposures with the 0.6-m CAT are binned three observations per point. The scatter of unbinned velocities is 11 m s$^{-1}$; the scatter of binned velocities is 6.2 m s$^{-1}$.

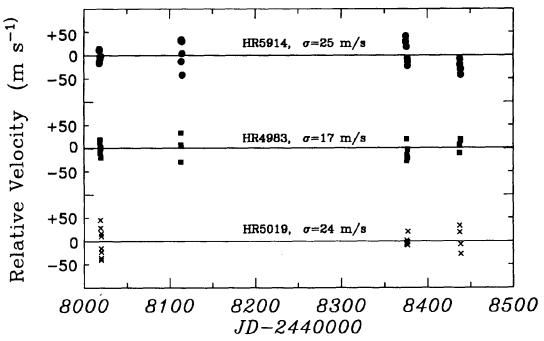


FIG. 3—Velocity tests for three solar-type stars, HR 5914, HR 4983, and HR 5019, spanning 1.2 yr. The scatter of 17–25 m s$^{-1}$ represents the precision obtained with the current preliminary Doppler analysis. Only about 1/5 of the available Doppler information was used in this analysis.

trum, centered on stellar absorption lines, are analyzed, each section yielding a Doppler shift via Eq. (1). Figure 1 displays the Doppler analysis in practice, showing a stellar template spectrum, $I_s$, the FTS $I_2$-cell transmission function, $T_{I_2}$, the model comprised of these two convolved with the PSF [the right-hand side (RHS) of Eq. (1)], and finally the actual observed spectrum through the absorption cell. At the bottom is the difference between the observed and model spectra. The typical rms of the residuals between model and observation is 0.6% of continuum, consistent with the S/N ratio of about 200 in each spectrum. The final Doppler shift is obtained from the average of the shifts of all stellar absorption lines. Relative weights are assigned to each Doppler shift according to Merline (1985) to account for the expected error from each line. Final velocities are obtained by correcting for the Earth's orbital and rotational velocity relative to the Solar-System barycenter (Stumpff 1980).

The cpu time required to process one echelle image on a SPARCstation 1+ is about 3 hr, including full reduction of the raw 2048×2048 CCD image, the determination of the PSF everywhere, and the Doppler modeling. Thus in the tests that follow, we restricted the Doppler analysis to only six spectral orders, containing only ~30 stellar absorption lines and only a few hundred iodine lines. This represents about 1/5 of the available Doppler information available to be fully utilized once a final analysis is established.

We have carried out several tests of the $I_2$-absorption-cell technique. We obtained 35 consecutive exposures (20 s each) of Arcturus during a 30-min period with the Coudé auxiliary telescope (CAT), a 0.6-m telescope that feeds the Lick 3-m telescope's echelle spectrometer. The resulting velocities had a standard deviation of 11 m s$^{-1}$, which evidently represents the current level of precision possible on this small telescope, albeit on the brightest stars. To check the randomness of the Arcturus velocities, we binned them in groups of three, and the resulting standard deviation dropped to 6.2 m s$^{-1}$. These velocities are shown in Fig. 2. Despite being obtained using a small telescope, this precision is comparable to the best reported (~13 m s$^{-1}$) on large telescopes (e.g., McMillan et al. 1985; Campbell et al. 1988; Cochran 1988). When we employ all spectral orders (five times more Doppler information) we expect to improve further on the 11 m s$^{-1}$ precision.

As another test of the $I_2$ technique, we made ~20 observations of three solar-type stars, HR 4983 (G0 V, $V$ =4.3), HR 5019 (G6 V, $V$=4.7), and HR 5914 (F9 V, $V$=4.6). The observations span 1.2 yr and were obtained on four different observing runs at the Lick 3-m telescope. The typical exposure times were only 5 min, achieving S/N=200 per pixel. Note that the typical exposure time by Campbell et al. (1988) to obtain precision velocities of these stars is 1 hr on the 3.6-m telescope at the Canada–France–Hawaii facility in Hawaii.

Figure 3 shows the relative velocities (arbitrary average) derived for these three stars. The scatter for the three stars is 17, 24, and 25 m s$^{-1}$, respectively. Thus, the precision of the echelle/$I_2$ technique appears to be ~25 m s$^{-1}$ long term, using only 1/5 of the available spectral information, and processed with only a preliminary Doppler analysis. For reference, Jupiter perturbs the Sun by 13 m s$^{-1}$.

We are aware of two sources of error that contribute to the observed long-term scatter of ~25 m s$^{-1}$. The signal-to-noise ratio of the spectra (~200) limits the precision with which the position of a line may be determined, as described by Merline (1985). Using his analysis, we anticipate a Doppler precision of about 100 m s$^{-1}$ per stellar absorption line. Since our current analysis incorporates 30 lines, the standard deviation of the mean is expected to be $100/\sqrt{30} = 18$ m s$^{-1}$. Since this is less than the observed scatter of ~25 m s$^{-1}$, another source of error likely persists. We suspect that this other error arises from inadequate extraction of the spectral PSF. The signature of this problem is that groups of lines that lie near each other on the CCD image occasionally give velocities that lie systematically away from the mean Doppler shift. These small systematic residuals may be due to inadequate determination of the PSF. Indeed, we currently represent the PSF with an analytic form consisting of the sum of three displaced Gaussians. We find that such a representation does not fit the wings of the PSF in some regions of the echelle format, causing discrepancies of about 1% (in terms of the peak intensity of the PSF). This inadequacy will be addressed in future versions by generalizing the analytical form of the PSF.

## 7. THE SCIENTIFIC PROGRAMS

### 7.1 Detection of Brown Dwarf and Planetary Companions

A major difficulty in astrophysics has been the detection of substellar objects, both brown dwarfs and planets, orbit-

ing other stars [for recent reviews, see Brown and Burrows (1990)]. Such objects bear on several diverse subfields of astronomy, such as: (1) the identification of dark matter both in the local Galactic disk (Bahcall and Flynn 1991) and in halos of other galaxies; (2) the understanding of protostellar fragmentation and protostellar disk evolution (Boss 1987; Shu et al. 1987); and (3) the incidence and characteristics of planetary systems.

Remarkably, there are no confirmed *bona fide* brown dwarfs known, although there are several interesting candidates: Gliese 569 (Forrest et al. 1988), GD 165 (Zuckerman and Becklin 1988; Becklin and Zuckerman 1988), and HD 114762 (Latham et al. 1989; Cochran et al. 1991). The lack of positive detections is noteworthy in light of the many searches, by different techniques, that have been sensitive to a broad range of parameter space (Boeshaar et al. 1986; Chester et al. 1986; Skrutskie et al. 1990; Zuckerman and Becklin 1987; Henry and McCarthy 1989). Similarly, there are no confirmed detections of *bona fide* extra-solar planets, although Campbell et al. (1988) have reported several candidates from possible velocity variations. The feasibility of detecting extra-solar planets with the *Hubble Space Telescope,* even with the optics repaired, is not promising (Brown and Burrows 1990).

Previous radial velocities by our group (Marcy and Moore 1989; Marcy and Benitz 1989) permitted the detection of companions with masses down to 10 $M_{\rm Jup}$ around 65 of the nearest stars, mostly M dwarfs. Despite this sensitivity, these velocities, coupled with astrometry of the same stars, have revealed no convincing substellar objects for orbital periods up to about 10 yr. Precise velocities by Campbell et al. (1988) for 12 main sequence stars have also revealed no brown dwarfs down to 10 $M_{\rm Jup}$. However, the work of Campbell et al., Latham et al., and Marcy and Benitz have revealed low-amplitude velocity variations that, if real, are indicative of companions of $\sim 10\ M_{\rm Jup}$ [cf., Marcy and Benitz (1989), Fig. 2, for Gliese 380]. The suggestion is that they are detecting either the tail of the brown-dwarf mass function near 10 $M_{\rm Jup}$, or the high-mass tip of the planetary mass function.

One may calculate the lowest detectable planetary mass from the so-called mass function,

$$\frac{M_2^3 \sin^3 i}{(M_1+M_2)^2} = \frac{P}{2\pi G}(1-e^2)^{3/2}K_1^3, \qquad (4)$$

where $M_1$ and $M_2$ are the masses of the primary and secondary, and $P$, $e$, and $K_1$ are the period, eccentricity, and velocity semiamplitude, respectively. The lowest detectable planetary mass $M_2$ corresponds to the minimum detectable velocity amplitude $K_1$.

We estimated the threshold value of $K_1$ by a series of Monte Carlo simulations of hypothetical binary orbits, assuming we made velocity measurements that had errors of 40 m s$^{-1}$. We choose 40 m s$^{-1}$ rather than the true uncertainty of $\sim$25 m s$^{-1}$ to demonstrate the science possible even with *somewhat inferior* precision. The artificial velocity curves spanned a wide range of assumed orbital parameters. For each of these artificial velocity curves, we computed the statistical significance of variation (simulating attempted detections) using the Scargle-periodogram analyses (Scargle 1982).

The minimum detectable companion mass, $M_{\rm min}$, is found to be

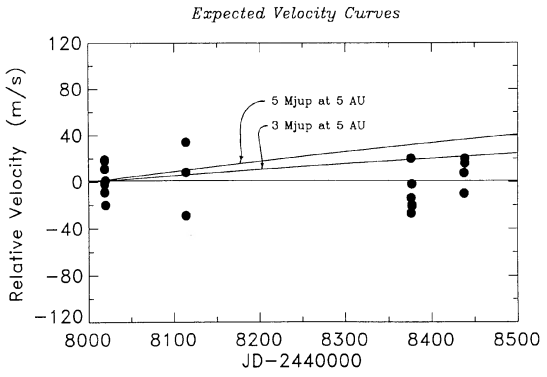


FIG. 4—Theoretical velocity curves for planets having 5 $M_{\rm Jup}$ and 3 $M_{\rm Jup}$, in circular orbits at 5 AU from a host G star. Overplotted are the actual velocities for HR 4983 (G6 V), showing the scatter typical of the current velocity precision. Only 1.2 yr is shown, the duration of the test observations. The current velocity precision marginally permits detection of a 3 $M_{\rm Jup}$ planet, but detection of a 1 $M_{\rm Jup}$ planet will require three times higher precision.

$$M_{\rm min} = 2.5 \frac{P_{\rm yr}^{1/3}}{\sin i} \quad (M_{\rm Jup}), \qquad (5)$$

where the dependence on $P$ and sin $i$ follows from Eq. (4), and the coefficient of 2.5 $M_{\rm Jup}$ is derived from the Monte Carlo tests. Thus, for moderate orbital periods, companions with masses of several $M_{\rm Jup}$ are detectable, even for a conservative estimate of errors, 40 m s$^{-1}$.

For longer orbital periods, astrometric detections of perturbations become increasingly sensitive, such as those carried out over decades at the Sproul, U.S. Naval, Allegheny, and McCormick Observatories. New astrometric techniques such as the MAP (Gatewood et al. 1986) and long-baseline optical interferometry (Shao et al. 1988) will improve the astrometric detectability by a factor of $\sim$10, thereby enabling corroborative planetary detections.

To illustrate the well-known problem involved in detection of extra-solar planets, Fig. 4 displays the *theoretical velocity curve* of a G main-sequence star perturbed by hypothetical planets having 5 and 3 $M_{\rm Jup}$, both in circular orbits of radius, 5 AU (12 yr period). Note that only a small portion of the velocity sine wave would be covered by our test observations after only 1.2 yr. We have overplotted the actual observed velocities for HR 4983 (from Fig. 3) for comparison. HR 4983 shows little evidence of velocity variations as large as those predicted for a 5 $M_{\rm Jup}$ planet, while detectability of a 3 $M_{\rm Jup}$ planet would be only marginally possible with the current velocity precision. Reflex velocity amplitudes vary linearly with companion mass as in Eq. (4). Thus, the detection of a 1 $M_{\rm Jup}$ planet at 5 AU would require an improvement in velocity precision of at least a factor of 3.

We have established a sample of 70 F-, G-, K-, and M-type main-sequence stars, including many of the stars observed for planet detection by Campbell et al. (1988), Cochran (1988), McMillan et al. (1985), and Gatewood et al. (1986). Precise velocities for the K and M main-sequence stars in the solar neighborhood are uniquely accessible by our system owing to the large wavelength coverage and throughput of the Lick echelle. (M dwarfs carry the advantage of low inertia, yielding twice the velocity

amplitudes of the G dwarfs for a given companion.) We plan to continue monitoring those M dwarfs that showed preliminary indications of velocity periodicity in the earlier, low-precision velocity survey (Marcy and Benitz 1989). Some of these, such as Gliese 380, show variations with amplitude of about 300 m $s^{-1}$, implying companions of about 10 $M_{Jup}$. These companions are easily verifiable with the $I_2$ technique. We also include in our sample some stars already known to possess interesting companions such as HD 114762 (Latham et al. 1989). A dynamical survey such as this will also reveal unseen, high-mass objects ($>1$ $M_{\odot}$) located tens of AU from the star since large reflex motion will occur.

Finally, we note that a critical problem historically has been the poor dependability of claimed detections of substellar companions. The sordid history need not be repeated if responsible corroborative observations are carried out, especially *independent* observations made with entirely different techniques (Brown 1989). We have carefully developed and applied such an approach in the analysis of Gliese 623 (Marcy and Moore 1989; McCarthy and Henry 1987) which incorporated astrometric and IR speckle interferometric observations, along with precision velocities. These three techniques provided not only mutual confirmation of the existence of the 80 $M_{Jup}$ companion, but also independent determination of the orbital parameters and hence the mass of the companion. Such a secure strategy will be even more viable with the development of more precise astrometric techniques, mentioned above, and the new speckle and IR imaging capabilities now available.

### 7.2 Cepheids and Stellar Seismology

Distances to Cepheids determined by the Baade–Weselink/Barnes–Evans method make use of the measured velocity variations to determine radius changes. However, the lines used in such measurements originate at widely different depths within the low-gravity Cepheid atmosphere. Thus, it has not been clear how to interpret the velocities obtained in such analyses. The solution lies in accurate kinematic modeling of the Cepheid atmosphere so that the line transfer and emergent fluxes can be properly calculated (Manduca and Bell 1981) as a function of phase.

We are developing an analysis to measure the velocities of a large number of lines in several Cepheids over full pulsation periods to detect systematic variations in velocity as a function of depth of line formation. This will involve use of the atmosphere line-transfer code of Bell, with the inclusion of a velocity field, to reproduce the observed line shifts and asymmetries. With the resulting kinematically justified atmospheric model, we intend to reapply the Baade-Weselink/Barnes-Evans methods to recalibrate distances to nearby Cepheids.

Finally, we note that Dr. S. Vogt and Dr. T. Brown have used the same iodine cell and echelle at Lick to detect stellar oscillations analogous to the 5 min solar oscillations. The expected amplitude for G and K dwarfs stars (integrated over all modes) is somewhat less than 1 m $s^{-1}$, less than the precision obtained to date with the $I_2$ cell. However, Fourier analysis permits extraction of embedded periodicities with amplitudes of about 1 m $s^{-1}$ (Brown 1990). An iodine cell for the Keck 10-m telescope will be constructed to pursue this oscillation effort.

Thanks are due to W. Livingstone and G. Ladd for assisting in the acquisition of the FTS iodine spectrum. Thanks are due Mylan Healy for glass-blowing the iodine cell. We received valuable assistance from Bruce Campbell, Jeff Valenti, Wayne Earthman, and Tony Misch. We acknowledge NSF Grant No. AST-8919634 to G.M. and the NASA Graduate Student Researchers Program fellowship to R.P.B.

## REFERENCES

Bahcall, J. N., and Flynn, C. 1991, preprint
Becklin, E. E., and Zuckerman, B. 1988, Nature, 336, 656
Boeshaar, P., Tyson, J. A., and Seitzer, P. 1986, in Astrophysics of Brown Dwarfs (Cambridge, Cambridge University Press), p. 76
Boss, A. P. 1987, ApJ, 319, 149
Brown, R. A. 1989, Progress in Extra-Solar Planet Detection, in Bioastronomy—The Next Steps, ed. G. Marx (Dordrecht, Kluwer), p. 117
Brown, R. A., and Burrows, C. J. 1990, Icarus, 87, 484.
Brown, T. M. 1990, ASP Conf. Ser., CCD's in Astronomy (San Francisco, ASP), Vol. 8, p. 335
Campbell, B., and Walker, G. A. H. 1979, PASP, 91, 540
Campbell, B., Walker, G. A. H., and Yang, S. 1988, ApJ, 331, 902
Chester, T. J., Fullmer, L. D., Beichman, C. A., Gillet, F. C., Low, F. J., and Neugebauer, G. 1986, BAAS, 18, 961
Cochran, W. D. 1988, ApJ, 334, 349
Cochran, W. D., and Hatzes, A. P. 1990, Proc. SPIE, 1318, 148
Cochran, W. D., Hatzes, A. P., and Hancock, T. J. 1991, ApJ, 380, L35
Deming, D., Espenak, F., Jennings, D. E., Brault, J. W., and Wagner, J. 1987, ApJ, 316, L771
Duquennoy, A., and Mayor, M. 1991, A&A, 248, 485
Forrest, W. J., Skrutskie, M. F., and Shure, M. 1988, ApJ, 330, L119
Gatewood, G., de Jong, J. K., Han, I., Stein, J., and Breakiron, L. 1986, Astrophysics of Brown Dwarfs (Cambridge, Cambridge University Press), p. 104
Geary, J. C., Torres, G., Latham, D., and Wyatt, W. F. 1990, ASP Conf. Ser., CCD's in Astronomy (San Francisco, ASP) p. 40
Gerstenkorn, S., and Luc, P. 1978, Atlas du Spectre d'Absorption de la Molecule de l'Iod (14800–20000 $cm^{-1}$) (Paris, C.N.R.S.)
Gilliland, R. L. 1990, Internal HST Technical Report: Deconvolution of Simulated HST Spectra. II. Extension to Variable PSF and New Techniques, 31 July 1990
Griffin, R. F., and Griffin, R. E. 1973, MNRAS, 162, 243
Heacox, W. D. 1988, in ASP Conf. Ser., Fiber Optics in Astronomy, ed. S. C. Barden (San Francisco, ASP), Vol. 3, p. 204
Henry, T., and McCarthy, D. W. 1989, ApJ, 350, 334
Koch, A., and Wohl, H. 1984, A&A, 134, 134
Latham, D. W., Mazeh, T., Stefanik, R. P., Mayor, M., and Burki, G. 1989, Nature, 339, 38
Manduca, A., and Bell, R. A. 1981, ApJ, 250, 306
Marcy, G. W., Lindsay, V., and Wilson, K. 1987, PASP, 99, 490
Marcy, G. W., and Moore, D. 1989, ApJ, 341, 961
Marcy, G. W., and Benitz, K. J. 1989, ApJ, 344, 441
McCarthy, D. W., and Henry, T. J. 1987, ApJ, 319, L93
Merline, W. J. 1985, in IAU Colloq., No. 88, Stellar Radial Velocities, ed. A. G. Philip and D. W. Latham (Schenectady, Davis), p. 87
McMillan, R. S. Smith, P. H., Frecker, J. E., Merline, W. J., and Perry, M. L. 1985, in IAU Colloq., No. 88, Stellar Radial Velocities, ed. A. G. Davis Phillip and D. W. Latham

(Schenectady, Davis), p. 63
Ramsey, L. W., Brown, T. M., Gilliland, R. L., and Noyes, R. W. 1990, in ASP Conf. Ser., Frontiers of Stellar Evolution, ed. D. Lambert (San Francisco, ASP)
Scargle, J. D. 1982, ApJ, 263, 835
Shao, M., et al. 1988, ApJ, 327, 905
Shu, F., Adams, F. C., and Lizano, S. 1987, ARAA, 25, 23
Skrutskie, M. F., Forrest, W. J., and Shure, M. 1990, AJ, 98, 1409
Smith, M. 1983, ApJ, 265, 325
Smith, P., McMillan, R., and Merline, W. J. 1987, ApJ, 317, L79
Stumpff, P. 1980, A&AS, 41, 1
Tarter, J. 1976, Ph.D. thesis, University of California, Berkeley
Wallace, L., Huang, Y. R., and Livingston, W. 1988, ApJ, 327, 399
Valenti, J. A., Butler, R. P., and Marcy, G. W. 1992, in preparation
Vogt, S. S. 1987, PASP, 99, 1214
Zuckerman, B., and Becklin, E. E. 1987, ApJ, 319, L99
Zuckerman, B., and Becklin, E. E. 1988, Nature, 330, 138